Warming Trends in the Arctic from Clear Sky Satellite Observations

JOSEFINO C. COMISO

NASA Goddard Space Flight Center, Greenbelt, Maryland

(Manuscript received 7 August 2002, in final form 25 April 2003)

ABSTRACT

Satellite thermal infrared data on surface temperatures provide pan-Arctic coverage from 1981 to 2001 during cloud-free conditions and reveal large warming anomalies in the 1990s compared to the 1980s and regional variability in the trend. The rms error of the derived surface temperatures when compared with in situ data ranges from 1.5 to 3 K over the 20-yr period. Average temperature trends are generally positive at 0.33 ± 0.16°C decade^{-1} over sea ice, 0.50 ± 0.22°C decade^{-1} over Eurasia, and 1.06 ± 0.22°C decade^{-1} over North America. The trend is slightly negative and insignificant at −0.09 ± 0.25°C decade^{-1} in Greenland with the negatives mainly at high elevations. The trends are also predominantly positive in spring, summer, and autumn causing the lengthening of the melt season by 10–17 days per decade while they are generally negative in winter. The longer-term in situ surface temperature data shows that the 20-yr trend is 8 times larger than the 100-yr trend suggesting a rapid acceleration in the warming that may be associated with the recent change in phase of the Arctic Oscillation that has been linked to increasing greenhouse gases in the atmosphere.

1. Introduction

The Arctic is expected to provide an early signal of global warming because of the amplification of the signal in the region due to feedback effects associated with the high albedo of snow and ice (Budyko 1966; Manabe et al. 1992). It is thus the appropriate region to examine the positive trends in global surface air temperatures reported previously (Raper et al. 1983; Hansen and Lebedeff 1987; Jones et al. 1999). Because of the paucity of station data in the Arctic and the presence of a dynamic sea ice cover, it has been difficult to assess quantitatively how surface temperature has been changing in the entire region. The lack of adequate temperature data north of 60°N latitude comes as no surprise because of the general inaccessibility of the Arctic, especially in winter. Some investigators have tried to remedy the situation by making use of data from buoys and meteorological stations since the late 1970s and apply spatial interpolations to fill in the gaps (Rigor et al. 2000). The resulting dataset from such an effort is a big improvement over previous records but some limitations in the interpolated data are apparent.

Arctic warming is suggested from recent reports of a retreating and thinning sea ice cover (Bjorgo et al. 1997; Parkinson et al. 1999; Rothrock et al. 1999; Wadhams and Davis 2000; Tucker et al. 2001). A rapidly declining perennial ice cover has also been reported recently (Comiso 2002) and 2002 has been cited as the year when the summer ice cover in the Arctic was least extensive during the satellite era (Serreze and Maslanik 2002, personal communication). To gain insight into this implied warming scenario through direct observations, two decades of satellite infrared data have been processed and analyzed in conjunction with in situ and other measurements. Under cloud-free conditions, infrared data provide skin depth (surface) temperatures and are shown to be generally consistent with surface air temperatures. The key source of historical surface temperature data is the Advanced Very High Resolution Radiometer (AVHRR) onboard National Oceanic and Atmospheric Administration satellites, which were processed as described previously (Comiso 2000, 2001). In this paper, we take advantage of such a truly global dataset to examine in spatial detail regional and interannual anomalies of surface temperature in the entire Arctic region, establish the spatial scope and persistence of such anomalies, and evaluate trends in surface temperature regionally and for the various seasons. Biases and possible effects on the trends, associated with having only cloud-free measurements, and interannual changes in cloud cover and aerosol are assessed.

2. Satellite observations of surface temperatures

When we think of global trends, we usually mean those that are derived from global averages. Such averages are more appropriately defined when obtained from satellite data that are able to provide large-scale

Corresponding author address: Dr. Josefino C. Comiso, NASA Goddard Space Flight Center, Oceans and Ice Branch, Code 971, Greenbelt, MD 20771.
E-mail: josefino.c.comiso@nasa.gov

synoptic and comprehensive observations of the entire region. Satellite thermal infrared data provide relatively accurate surface temperatures because the infrared emissivities of most surfaces (e.g., water, snow, and ice) are spatially uniform and close to unity. However, since infrared radiation is sensitive to clouds, surface measurements can be derived only during cloud-free conditions. A special cloud-masking technique had to be utilized in the processing of Arctic data because snow-covered surfaces and clouds have similar infrared signatures. In addition to the use of conventional thresholding techniques, a daily differencing technique was developed, as reported in Comiso (2000), by taking advantage of the large daily variability in the spatial distribution of clouds. The dataset provides detailed information about the distribution of surface temperature and has been successfully used to identify cooling trends in Antarctica (Comiso 2000) that were recently confirmed by studies using in situ data (Doran et al. 2002). The AVHRR temperature dataset has also been used successfully in spatially detailed correlation studies of Antarctic surface temperatures with Southern Oscillation indices and the climate anomaly in the Antarctic peninsula (e.g., Kwok and Comiso 2002; King and Comiso 2003).

To illustrate the effectiveness in reproducing surface temperatures from AVHRR data in the Northern Hemisphere, we make use of accurate in situ surface temperature datasets that have recently become available. One of these sets consists of surface temperatures acquired during the 1-yr-long ice station project Surface Heat Budget in the Arctic (SHEBA) (Perovich and Elder 2001) conducted in the central Arctic from October 1997 through September 1998. A comparison of these data with corresponding AVHRR data is shown in Fig. 1a and the results indicate good agreement, with an rms error of 1.58°C and a correlation coefficient of 0.992. These results are especially encouraging since both measurements in Fig. 1a reflect the temperature of a thin layer on the snow/ice surface during cloud-free conditions.

Clouds can cause a statistical bias on the monthly averages derived from AVHRR data. To quantify the magnitude of the cloud effect, we made use of continuous surface temperature measurements (with and without clouds) observed at the SHEBA station during September 1997 to October 1998. Actual monthly surface temperatures (i.e., combining cloudy and cloud-free surface data) are calculated and compared with monthly surface temperatures of cloud-free data only (with the cloud cover determined by the AVHRR data) and the results are presented in Fig. 1b. The results show a good agreement of the two monthly temperatures with a correlation coefficient of 0.997 and an rms error of 0.95°C. The average difference is about 0.07°C with the difference being negative at −0.27°C in autumn and −0.44°C in winter and positive at 0.94°C in spring and 0.03°C in summer. The negative values in autumn and winter

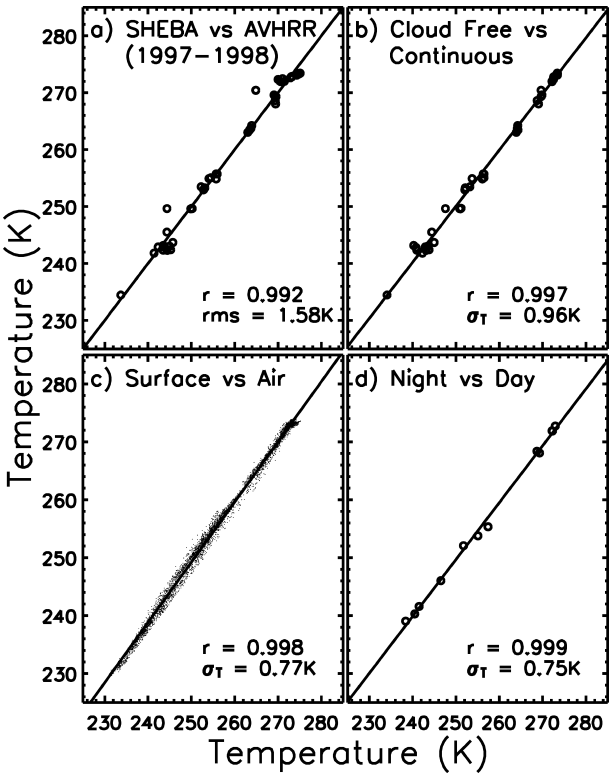

FIG. 1. Comparison studies using primarily SHEBA in situ data from Oct 1997 to Sep 1998: (a) AVHRR vs SHEBA monthly surface temperature data, (b) monthly cloud-free surface temperatures vs real (continuous) monthly surface temperatures, (c) monthly surface temperatures vs monthly surface air temperatures, and (d) monthly night data vs monthly day data.

may be a result of an atmospheric inversion, which is known to be prevalent during the period. In Greenland, the yearly average is −0.66°C consistent with similar studies in the Antarctic and stronger inversion effects at high elevations.

Most of the global in situ surface temperature data are 2-m air temperatures recorded mainly at meteorological stations around the world. The 2-m air temperature provides a good estimate of surface temperature but the two temperatures can differ significantly depending on surface material and atmospheric conditions. Fortuitously, the year-long SHEBA daily data have both 2-m air temperature and surface temperature and can be used to gain insights into the difference between the two temperatures. The result of a comparative analysis is presented in Fig. 1c. The two variables are strongly correlated, as expected, with a correlation coefficient of 0.998 and an rms error of 1°C. The air temperature is generally greater than that of the surface temperature by about 0.95°, 0.26°, 0.13°, and 0.13°C for winter, spring, summer, and autumn, respectively, the average being 0.34°C, which is within the retrieval error for the AVHRR temperatures. A regression analysis of the data points in Fig. 1c provides a transformation equation of

$$T_S = -10.592 + 1.0392\ T_A, \quad (1)$$

where T_S and T_A are surface and air temperatures, respectively. A similar study using the same set of variables observed in the high elevations of the Greenland Ice Sheet from 1995 through 2000 (Steffen and Box 2001) shows similar magnitude in effects but opposite in sign, being −0.49°, −0.26°, −0.76°, and −0.36°C for winter, spring, summer, and autumn, respectively, and an average of −0.36°C. The cause of this difference is not well understood but may in part be due to atmospheric inversions as indicated earlier. For completeness, monthly averaged temperatures observed during descending orbits (night) are compared with similar temperatures during ascending orbits (day) and the correlation coefficient is 0.999 with a standard deviation of 0.85°C. The yearly average for night data is colder than those of day, as expected, but only by about 0.5°C.

To study the interannual consistency of the AVHRR data we compared the latter with in situ data during the 1981–2000 period. One of the most comprehensive datasets that have been put together for Arctic surface air temperatures is that for the International Arctic Buoy Program and Polar Exchange at the Sea Surface (IABP/POLES) project (Rigor et al. 2000). The data compiled are generally surface air temperatures from buoys and meteorological stations around the Arctic but mapped for the entire Arctic region using a special interpolation scheme. These data are first converted to surface temperatures using the transformation equation above and then compared with corresponding AVHRR maps. The two maps are generally coherent and in good agreement except in some interpolated areas and during the summer. The disagreements in summer are in part because IABP/POLES data show melting temperatures in basically the entire Arctic region during the summer period for all years as in the modeling study by Lindsay (1998). On the other hand, AVHRR data show significant interannual changes in the length and coverage of summer melt, as presented in section 4. To gain insights into the discrepancies between the two datasets, subsets of the IABP/POLES data are compared with AVHRR data in areas that include meteorological stations and the results are presented in Figs. 2a, 2b, and 2c for Alaska (Pt. Barrow), Siberia, and Franz Josef Land, respectively. The size of these study areas are 2.28, 4.16, and 1.52 $\times$ 10^5 km^2 centered at (71.1°N, 202.5°E), (77.7°N, 133.5°E), and (80.6°N, 53.1°E), respectively. The datasets are shown to be highly correlated with correlation coefficients of 0.988, 0.985, and 0.992, and rms errors of 2.0, 2.4, and 2.5 K, respectively, for Alaska, Siberia, and Franz Josef Land. These results indicate that when real surface (not interpolated) data are compared, the two datasets are generally in good agreement. Since the data plotted in Figs. 2a, 2b, and 2c are monthly data for the period from 1981 to 1999, the results also show that the AVHRR data are temporally consistent despite the use of data from different AVHRR sensors to put together the historical time series.

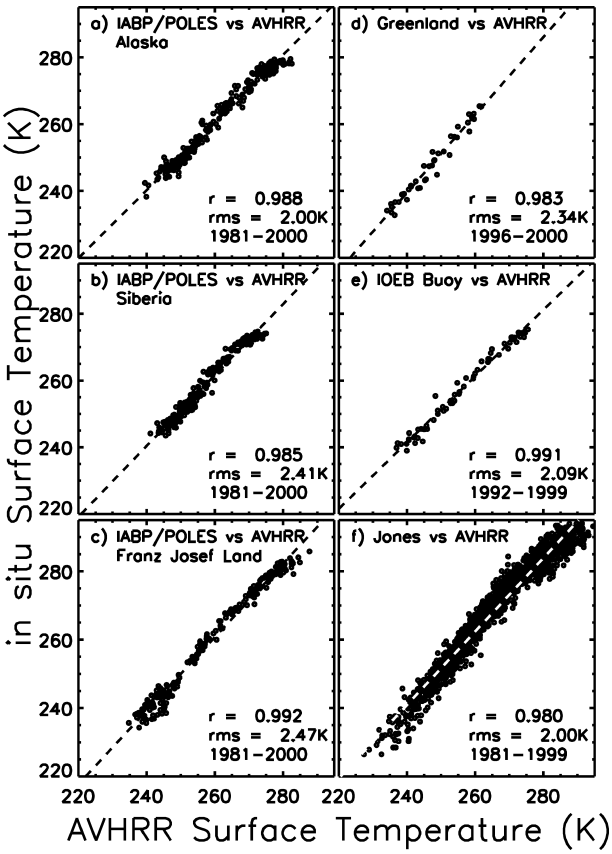

FIG. 2. Comparison studies of IAOB/POLES vs AVHRR at three selected regions: (a) Point Barrow in Alaska, (b) parts of Siberia, and (c) Franz Josef Land. Also, comparison studies of (d) Greenland ice sheet vs AVHRR data, (e) IOEB buoy vs AVHRR data, and (f) Jones dataset vs AVHRR data.

Among the other datasets compared with AVHRR data are the recently available and well-calibrated data from the Greenland ice sheet (Steffen and Box 2001). The scatterplot in Fig. 2d shows good consistency of the AVHRR data with the Greenland data for the period 1996–2000 (Fig. 2d) with a correlation coefficient of 0.983 and an rms error of 2.34 K. Another good dataset over the central Artic is that collected during the International Ocean Environmental Buoy (IOEB) program over the period from 1992 to 1998 (Honjo et al. 1995). The AVHRR data again shows good agreement with the IOEB temperatures (Fig. 2e) with a correlation coefficient of 0.991 and an rms error of 2.1 K. Finally, we compared AVHRR data from 1981 to 1999 with an updated version of data compiled by Jones et al. (1999). The result (Fig. 2f) shows good agreement with a correlation coefficient of 0.980 and an rms error of 2.0 K.

In the aforementioned and other comparisons, the rms errors range from 1.5 to 3 K. This is generally consistent, if not better than previous estimates for the AVHRR data (Steffen et al. 1993). Considering that the seasonal

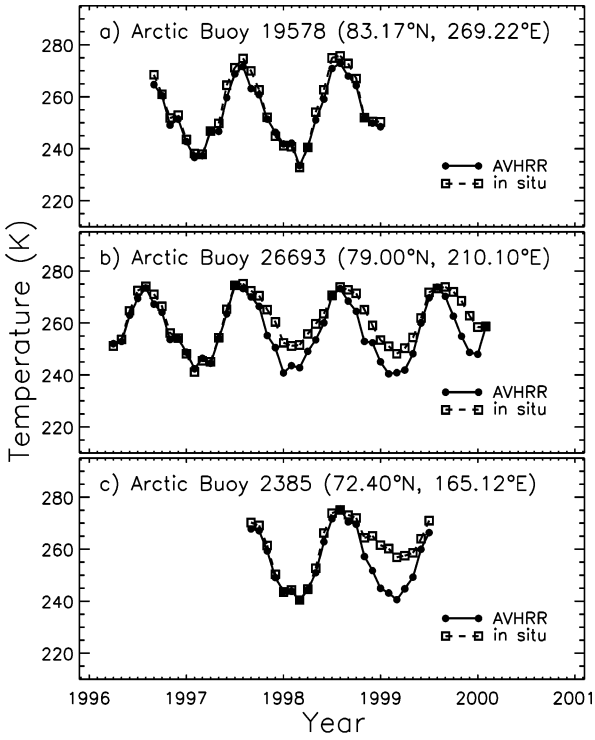

FIG. 3. Comparison of AVHRR and Argus buoy monthly temperatures for (a) buoy #19578, (b) buoy #26693, and (c) buoy #2385.

and spatial fluctuations are as high as 35°C in the ice-covered Arctic region (compared to 3°C for the oceans), our satellite data provide the accuracy needed to detect spatial and interannual changes in Arctic surface temperatures. It should be pointed out that disagreements are not necessarily caused by retrieval problems with AVHRR data since in situ surface measurements in polar regions can be affected by adverse weather conditions. To cite some examples, month-to-month comparisons of AVHRR data with Arctic Argus buoy data (used in the compilation of the IABP/POLES dataset) are shown in Fig. 3. In Fig. 3a, the AVHRR data are shown to be consistent with Arctic Argus buoy #19578 during the lifetime of the buoy, while a similar comparison with Argus buoy #26693 in Fig. 3b shows good agreement during the first year and a half but significant differences during subsequent years. In the latter case, the AVHRR values are shown to be more realistic since they agree better with expected winter values as indicated in the previous year. It is possible that the buoy sensor was buried by snow after the first year of operation and therefore the measurement may represent the warmer snow temperature in winter instead of surface temperature. A similar case also occurred with Argus buoy #2385 as shown in Fig. 3c. It is thus possible that the actual rms error in the AVHRR data is even better than what is estimated in the aforementioned comparative analysis.

To assess interannual variability of surface temperatures in the Arctic, yearly averages were generated in map format. The averaging was done for the time interval from August of one year to July the following year to cover an entire sea ice season. Such annual averages are generated instead of averages over each calendar year because surface temperature and ice extent are strongly coupled (Jacobs and Comiso 1997) and such data could provide insights into the observed interannual changes in the ice cover (Bjorgo et al. 1997; Parkinson et al. 1999; Comiso 2002). This makes the data consistent and easier to compare with similar averages in the Antarctic. These yearly averages were used to generate color-coded yearly anomaly maps (Fig. 4) for the period from August 1981 to July 2001. The anomaly maps were generated by taking the difference of each annual average and the climatology (average of the 20 yr of data). The color codes are such that the yellows, oranges, reds, and burgundys represent anomalously warm (positive) regions while the grays, greens, blues, and violets represent anomalously cold (negative) regions. The maps provide spatially detailed features and allow easy identification of locations of highly positive or negative temperature anomalies during each year. At a glance, it is apparent that there is a predominance of cold anomalies in the 1980s while warm anomalies were dominant starting in 1989 up to 2000. This phenomenon alone is already a good indication that the recent decade was warmer than the earlier one in much of the Arctic region. Similar results were observed for some months of the year at 925-hPa by Overland et al. (2002) in the western Arctic. Also, the distinct change from the generally negative to positive temperature anomalies coincides with the observed shift in the Arctic Oscillation from the 1979–98 period to the 1989–98 period (Rigor et al. 2002).

Large year-to-year changes in the spatial temperature distributions are revealed by the yearly anomaly maps. The coldest temperature in the Arctic Basin is shown to occur during the 1986–87 period whereas the warmest occurred during the 1999–2000 period. The Greenland ice sheet is also shown to have its coldest temperature during the 1991–93 period, which may in part be associated with the Mount Pinatubo eruption in 1991. Also, there was a general warming in the Barents Sea and Greenland and a cooling everywhere else in the 1984–85 period while it is almost exactly the opposite scenario in 1992–93. During the El Niño Southern Oscillation (ENSO) period of 1997/98 the temperature anomalies were very positive in the western (North American) region, while negative anomalies are apparent in the eastern (Eurasian) region. Furthermore, the warm anomalies expanded from just the western section in the 1997–98 period to the entire Arctic basin during the 1999–2000 period.

The spatial and interannual variability in the anomalies are caused in part by the ever changing atmospheric circulation (Mysak and Venegas 1998), which at times is cyclonic and at other times anticyclonic (Proshutinsky

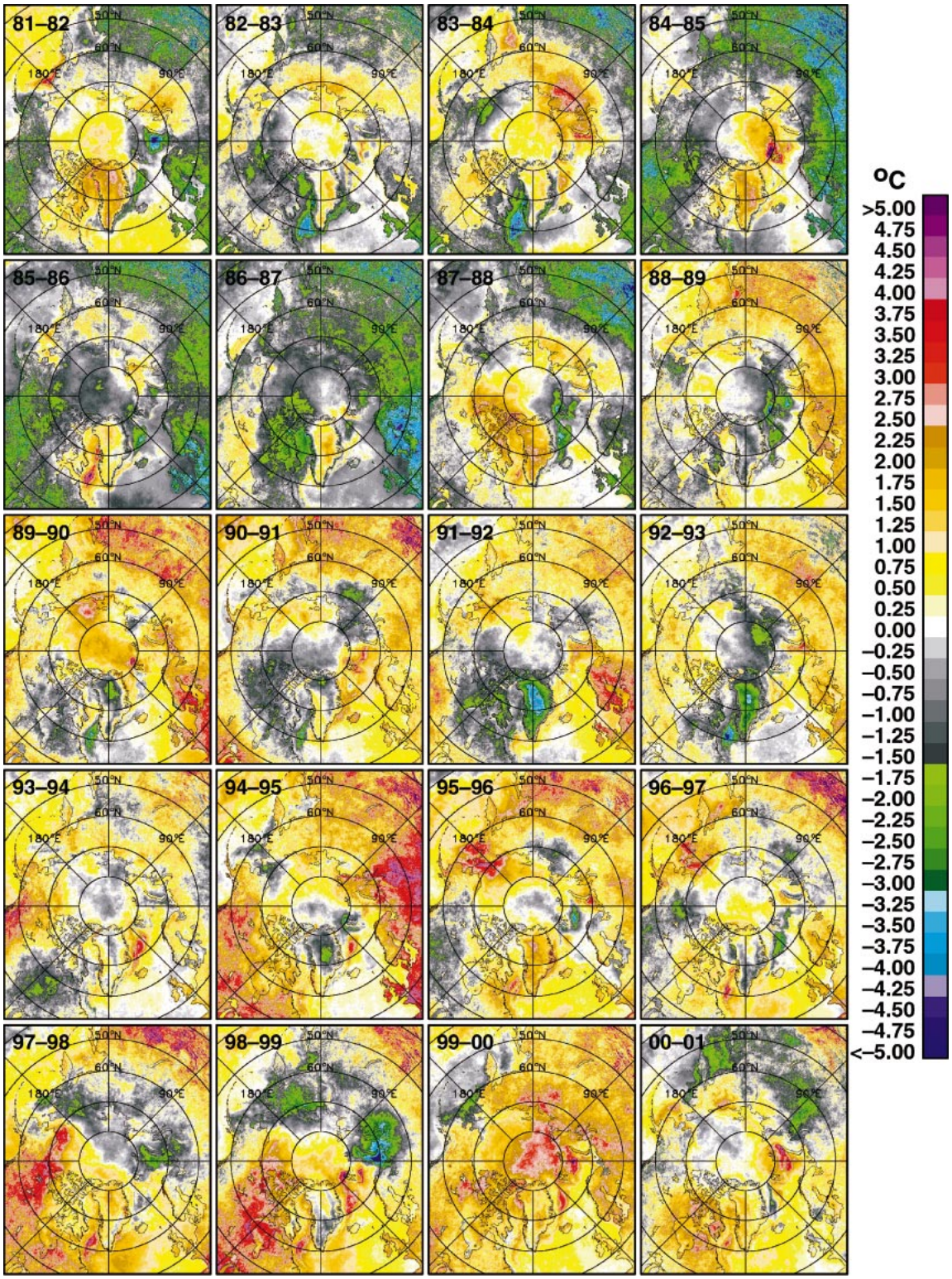

FIG. 4. Color-coded yearly anomalies in temperatures derived from AVHRR data from Aug 1981 to Jul 2001. The yearly averages make use of data from Aug of one year to Jul the following year to match the yearly growth and decay period of sea ice. The anomalies were calculated by subtracting the yearly climatology (1981–2001) from each of the yearly temperature averages.

and Johnson 1997). Examination of European Centre for Medium-Range Weather Forecasts (ECMWF) wind data in the 1990s indicates a reversal in wind circulation from the year 1995–96 to the 1997–98 period (results not shown, but similar results were reported by Overland et al. 2002) that may indeed be associated with the observed change in the polarity of the temperature anomaly in the Beaufort/Chukchi Seas. The impact of decadal changes in the pressure data and associated changes in wind directions caused by the weakening of the Beaufort high pressure cell and the strengthening of the European low pressure cell has been cited as a factor in the changes in surface temperature (Walsh et al. 1996; Mysak and Venegas 1998). Such changes are reflected in the difference (in sign) of the anomalies in the 1980s compared to those in the 1990s as mentioned previously.

3. Trends in the Arctic surface temperature

To put the anomaly maps discussed in the previous section in better perspective, trends in surface temperature were calculated on a pixel-by-pixel basis and the results for the pan-Arctic region are presented in Fig. 5a. The data used for this trend analysis are monthly anomaly data from August 1981 to July 2001 derived by subtracting the monthly climatology from each data element of each monthly temperature. The trends were also calculated using the yearly averages and the resulting trend map (not shown) is very similar but less accurate than that shown in Fig. 5a. The statistical errors of the trends, shown in Fig. 5b, are generally less than 0.3°C decade^{-1} in the central Arctic Ocean and increase gradually in the peripheral seas. The spatial distribution of the errors is shown to be very different from that of the trends indicating that errors in the trend are not amplified when the trend values are high. The standard deviations of the anomalies in each pixel (not shown) were found to range from 2.8° to 4.0°C and are spatially coherent with the statistical errors.

It is interesting to note that the trends in Arctic region (>60°N) show large spatial variability with relatively high positive values observed in northern Canada, Alaska, and the Beaufort Sea while negatives values are located in the eastern Bering Sea and parts of Russia. The spatial distribution of the trends is coherent with regional changes in the sea ice cover in the Northern Hemisphere as previously reported. For example, negative trends in the Bering Sea are consistent with positive trends in the sea ice cover in the same region while the positive trends that extend from the Chukchi and Beaufort Seas to the Canadian Archipelago and northern Canada are correlated with the observed decline of the sea ice cover in the same general location (Parkinson et al. 1999). The temperature anomalies, however, provide more information than the sea ice cover anomalies since the former depicts in good spatial detail the scope of warming beyond the sea ice cover. It is intuitively surprising that the trend values become negative at the summit of the Greenland ice cap, since the neighboring areas are generally positive. The trends are coherent with the observed thickening at high elevations and thinning at low elevations in Greenland (Krabill et al. 2000). At low elevations, the trends are positive but the thinning may in part be due to the changing dynamics of the ice sheet as discussed by Zwally et al. (2002).

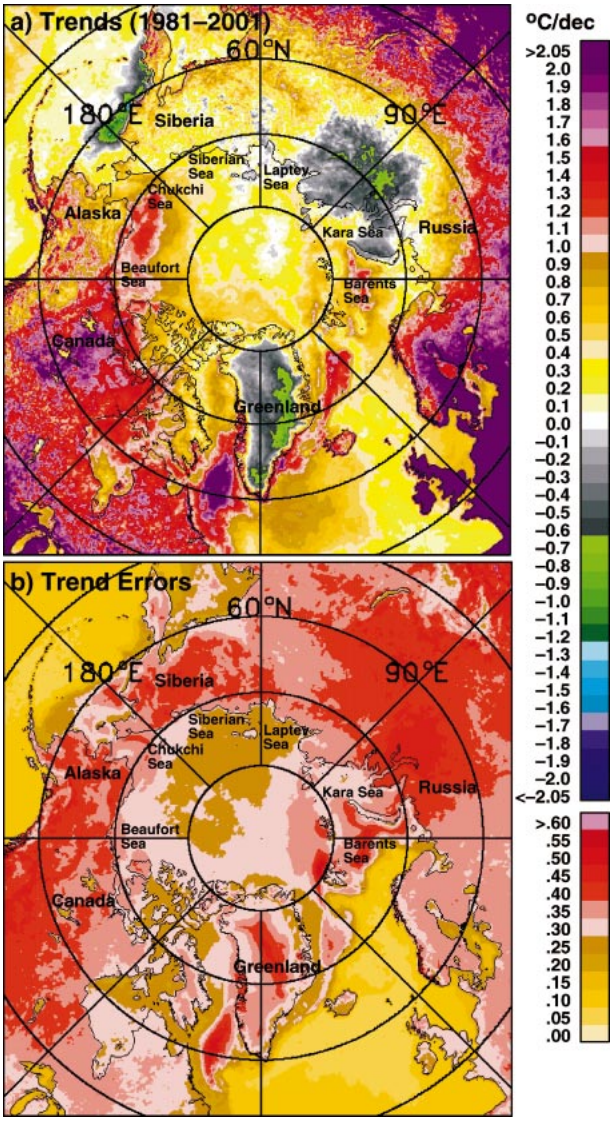

FIG. 5. (a) Color-coded trend map for the entire Arctic, and (b) statistical error of trends. Trends are derived through linear regression of monthly anomalies in each data element from 1981 to 2001. The anomalies are calculated by subtracting monthly climatology from the monthly values.

To quantitatively evaluate the trends on a regional basis, mean values of monthly anomalies over sea ice, Greenland, and areas located above 60°N in North America and Eurasia were calculated and results are shown in Fig. 6. Trends over sea ice are not easy to interpret because of changing percent and location of open water within the ice pack. To minimize uncertain-

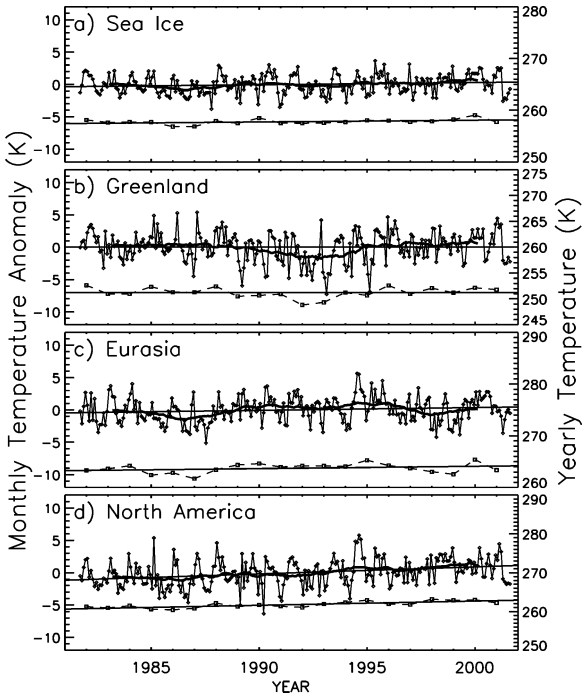

FIG. 6. Plots of average trends over (a) sea ice-covered areas with ice concentration>80%, (b) Greenland, (c) North America (north of 60°N), and (d) Eurasia (north of 60°N).

ties in the average trend in the region, Fig. 6a reflects only sea ice covered areas with concentrations greater than 80%. The average surface temperature over sea ice data is shown to be increasing at the rate of 0.34 ± 0.16°C decade^{-1}. Following the technique used in Draper and Smith (1981), the 95% confidence level for this trend is between 0.019° and 0.66°C decade^{-1}. Similar analysis was done using higher ice concentration thresholds (e.g., 90%) and the trend results (not shown) are basically the same. A slightly negative but insignificant trend is found over Greenland (Fig. 6b) where the rate is −0.02 ± 0.25°C decade^{-1} but the cooling is mainly at high elevations while warming trends are observed around the periphery. These results are consistent with recent reports on mass balance and peripheral thinning in the Greenland ice sheet (Krabill et al. 2000; Thomas et al. 2000). It is interesting to note that cooling is also reported at the high elevations in the Antarctic (Comiso 2000; Doran et al. 2002) over approximately the same period.

The average trend is relatively high in Eurasia (Fig. 6c) at 0.43 ± 0.22°C decade^{-1}, but the highest regional trend actually occurred in North America (Fig. 6d) at 1.09 ± 0.22°C decade^{-1}. The 95% confidence level for the trend over North America is between 0.65° and 1.53°C decade^{-1} while that over Eurasia is between 0.09° and 0.86°C decade^{-1}. The trend for Eurasia is consistent with that derived for meteorological stations (as described in the following section) located primarily in the same general region. Yearly averages are also shown in Fig. 6 and the trends from the yearly data are practically identical to those of the monthly anomalies but are not statistically as accurate.

The unique environment in the Arctic makes it important that the trends are also assessed on a season by season basis. The Arctic region is predominantly covered by snow and ice, the seasonal extent of which can vary significantly from one year to another depending on changes in surface temperatures. The seasonality in the trends is depicted in spatial detail in the trend maps in Fig. 7. The maps show that the trends are very different in different areas for the different seasons but are generally positive except in winter. The trend map in autumn (Fig. 7a) shows that the most positive trend inside 60°N occurs north of Alaska in the Chukchi Sea and Beaufort Sea regions but this is caused in part by retreats in the ice cover in the 1990s as described previously (McPhee et al. 1998; Comiso 2001). During this season, there is a general warming in the entire Arctic basin including North America and the periphery of Greenland, while there appears to be a cooling in parts of northern Russia, especially between 85° and 100°E. In the winter, warming is confined to North America, Europe, and the Beaufort Sea region while cooling is apparent in Alaska, Bering Sea, Chukchi Sea, Siberia, and a large part of the Arctic basin. This cooling trend in much of the Arctic during winter is consistent with positive trends in ice extent for the same season of about 1%–8% decade^{-1} in sea ice areas observed in the Arctic Ocean, Canadian Archipelago, and Bering Sea (Parkinson et al. 1999). The winter results do not appear to be consistent with Rigor et al. (2000) but mainly because the trends in the latter are for a different time period. Analysis of IABP/POLES dataset for the same time period (i.e., 1981–2000) yielded similar trend patterns (not shown) including the cooling trends mentioned above. In spring, significant warming occurs north of Greenland, Alaska, Beaufort Sea, and the Canadian peninsula. It is interesting to note that areas with high warming trends over sea ice generally correspond to areas covered by thick multiyear ice floes in the western region (McPhee et al. 1998) that has been observed to be declining (Johannessen et al. 1999; Comiso 2002). In the summer, there is an apparent warming practically everywhere, except in Greenland. These results are again inconsistent with those of Rigor et al. (2000) in which the trend is practically zero everywhere in the Arctic basin. Further studies are needed to resolve the discrepancies mainly because of the lack of adequate in situ data. Suffice it to say for now that a summer warming is consistent with an increasing length of the melt season as presented in the following section and a rapidly decreasing perennial ice cover (Comiso 2002).

Quantitatively, average temperature trends over sea ice are 0.59 ± 0.35°C decade^{-1} in autumn, −0.89 ± 0.34°C decade^{-1} in winter, 0.55 ± 0.28°C decade^{-1} in spring, and 1.22 ± 0.25°C decade^{-1} in summer. The seasonal trends indeed suggest an earlier spring melt, a

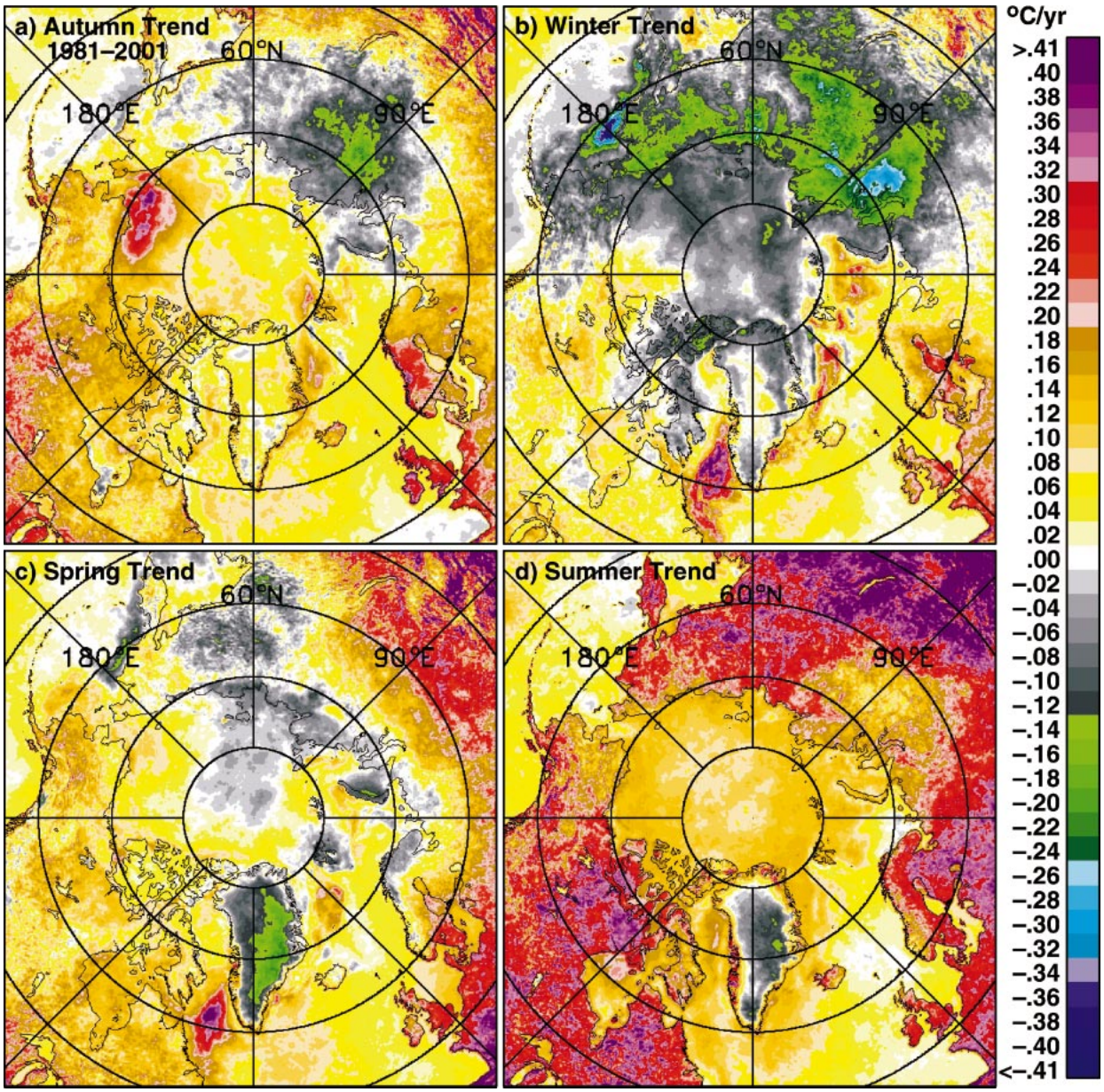

FIG. 7. Color-coded trend maps for the Arctic in (a) winter (DJF), (b) spring (MAM), (c) summer (JJA), and (d) autumn (SON) for the period 1981–2000.

warmer summer, and a later freezeup in autumn all corresponding to an increased ice melt period and suggesting a declining volume for sea ice (Häkkinen and Mellor 1990). The 95% confidence in the trend is between −0.21° and 1.21° for the autumn, between −1.57° and −0.21° for the winter, between −0.01° and 1.11° for the spring, and between 0.71° and 1.73°C decade^{-1} for the summer. The most important of these trend results is likely the summer warming trend, which together with the spring and autumn warming trends can cause significant impacts on the perennial ice regions.

It should be noted as well, that the monthly anomalies are quite variable with deviations from the mean as large as ±5°C. The variability is high over North America where the trend is most positive and in Greenland where the trend is slightly negative. It is least variable over the sea ice region. Such variability reflects in part the interannual changes in the onset of melt or freezeup.

4. Length of the melt period

In sea ice–covered areas, the melt season starts when the ice temperature gets to be 271 K or higher and ends when the ice temperature gets back to 271 or lower.

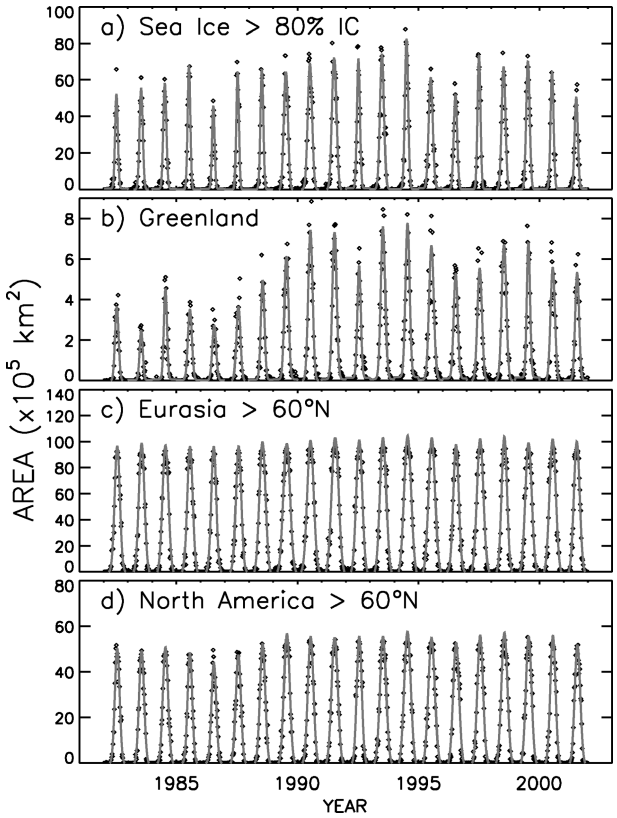

FIG. 8. Weekly areas with temperatures greater than 270 K to estimate melt areas over (a) sea ice, (b) Greenland, (c) Eurasia, and (d) North America. Gray line represents Gaussian fits to the monthly data points for each year.

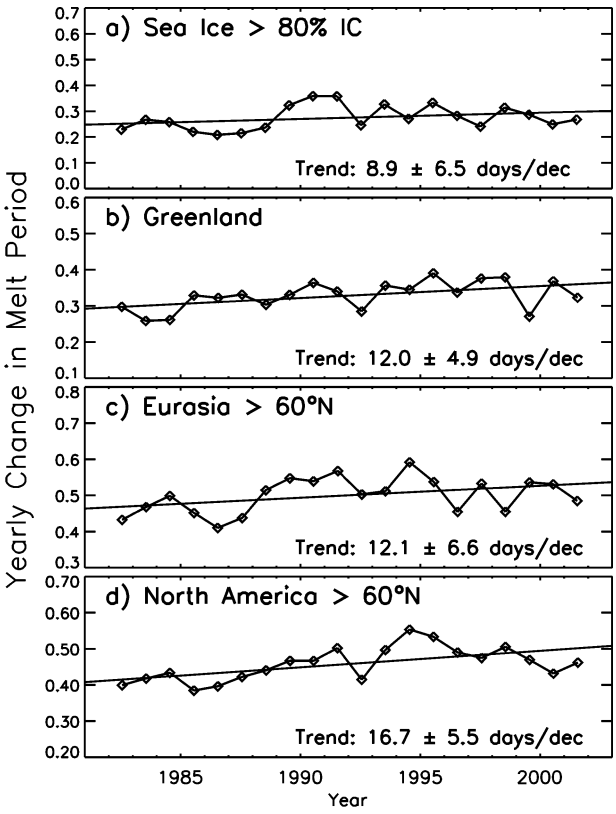

FIG. 9. Length of the melt season estimated using 4σ (standard deviation determined from the Gaussian fit parameters) for each year over (a) sea ice, (b) Greenland, (c) Eurasia, and (d) North America.

Over land, the melt season starts and ends at 273 K (the freezing temperature of freshwater) instead of 271 K. To be able to detect yearly variability in the length of the melt period, weekly averages were used, instead of monthly averages since a higher temporal variability than the latter is needed to detect the changes. Small gaps in the weekly data due to the cloud masking were observed but mainly in regions south of 50°N and were filled in by a mixture of simple spatial and temporal interpolation. The surface area with temperatures at or above melt temperatures (minus 1 K to account for errors in the retrieval) are quantified separately for the various regions in the Arctic (>60°N) and the results are shown for the four study regions in Fig. 8. The distributions show rapid increases in melt area in spring and summer followed by rapid decreases in autumn. Interannual changes in the distribution are apparent especially over Greenland where melting occurs at a small fraction of the total area. To quantify yearly changes, a Gaussian function was fitted on the weekly distribution for each year and the results are represented by the gray lines (Fig. 8). The fitted Gaussian provides a good representation of the evolution of the area of surface melt during the melt season. One of the fit parameters, σ, which is approximately half the width of the Gaussian curve, is used to provide a statistically consistent means to assess changes from one year to another. In our analysis, we simply use 4σ to represent the length of the melt period. This minimizes the errors in determining the actual onset of melt and of freezeup associated with large fluctuations in temperature during the initial and final part of the record. The time dependence of 4σ for the various study regions is depicted in Fig. 9, which shows large regional and interannual variability of melt seasons. Regression analysis on the data points indicates that the length of melt has been increasing by 9 ± 7, 12 ± 5, 12 ± 7, and 17 ± 6 days decade^{-1} over sea ice, Greenland, Eurasia, and North America, respectively. The impact of an increase in the melt period by 9–17 days can be substantial, especially over sea ice (Hakkinnen and Mellor 1990; Lemke and Hilmer 2000) and the ice sheets (Zwally and Fiegles 1994). In Eurasia and North America where the trends are highest, the peak values occurred in 1994 while in Greenland, it occurred in 1995. It is also interesting that despite overall cooling in Greenland as discussed in the previous section, the length of the melt period has been increasing at a fairly rapid rate. The observed cooling is mainly at high elevations while at the melt zone, the ice sheet thickness has actually been decreasing. Again, these results are consistent with recent studies on the Greenland

TABLE 1. Percentages and trends in cloud cover (1981–2000) in various regions and seasons of the Northern Hemisphere.

Region	Autumn		Winter		Spring		Summer	
	%Clouds	Δ%decade^{-1}	%Clouds	Δ%decade^{-1}	%Clouds	Δ%decade^{-1}	%Clouds	Δ%decade^{-1}
Sea ice (IC > 80%)	66.6	−3.4	67.9	−5.4	66.0	−1.3	65.2	−1.5
Greenland	75.8	−2.1	75.4	−3.4	75.8	−0.7	78.4	3.0
Eurasia (>60°N)	77.5	−3.3	76.7	−5.2	75.8	−2.7	82.7	−1.3
North America (>60°N)	77.6	−3.5	74.4	−5.5	75.3	−2.6	85.0	−1.9

ice sheet (Krabill et al. 2000; Thomas et al. 2000). An increasing melt period may also cause an even more profound effect since surface melt has been observed to cause an acceleration of the ice sheet flow in Greenland (Zwally et al. 2002).

5. Sources of errors in the variability and trend analysis

a. Interannual variability of clouds and aerosols

Interannual variations in the fraction of cloud cover in the Arctic may impact the accuracy of observed trends in surface temperatures since only clear sky AVHRR data are used. To gain insights into this phenomenon, we generated monthly and yearly averages of the fractions of cloud cover from the AVHRR data for the different study regions. The averages of these fractions on a season by season basis are given in Table 1. The monthly data are also used to create monthly anomalies and yearly anomalies in cloud cover (Fig. 10) that are in turn used to evaluate the cloud variability and trend. The results from both monthly anomaly and yearly data show negative trends of about −3% decade^{-1} for all regions except for Greenland where the trend is less negative at −0.8% decade^{-1}. The few percent change per decade may be significant since the fraction of clouds in the Arctic is high averaging about 75%. To evaluate the effect of a few percent change in cloud cover to the cloud-free temperature trend, we use the mixing equation:

$$T_S = F_C T_{SC} + F_N T_{SN}, \quad (2)$$

where T_S is the actual surface temperature for the region, T_{SC} is the surface temperature in cloudy areas, T_{SN} is the surface temperature in no-cloud areas, F_C is the fraction of cloud-covered areas, and F_N is the fraction of areas not covered by clouds. For a typical case of 75% clouds, a surface temperature of 265 K for cloud-covered areas, and a temperature of 264.5 K for cloud-free areas, a trend in cloud cover of 3% decade^{-1} would cause a trend of 0.045°C decade^{-1} on cloud-free temperature trend. Such a change is very small compared to the aforementioned trends in cloud-free temperatures from AVHRR data. It should be pointed out that despite the large percentage of cloud cover, the cloud-free temperature data fills up much of the Arctic region on a daily basis because of the high sampling rate of the orbital data and the fact that clouds are continually on the move.

Another factor that can affect trend results is the changing aerosol concentration in the Arctic. The impact of the increase in aerosol during the Mt. Pinatubo volcanic eruption on the Greenland ice sheet temperature has been noted earlier. Aerosol particles affect solar and terrestrial radiation through scattering and absorption and also the microphysical and optical properties of clouds through their role as condensation nuclei. There are some stations in the Arctic [e.g., the Atmospheric Radiation Measurement (ARM) site at Barrow, Alaska] where measurements have been made and results show that total scattering from aerosols has been decreasing at 2% yr^{-1} since 1980 while the concentration of condensation nuclei has been increasing at 3% yr^{-1}. The impact of scattering is to reduce the temperature observed by the AVHRR sensor but this is partially compensated by emissions from the aerosol particles. The overall impact of such changes in aerosol concen-

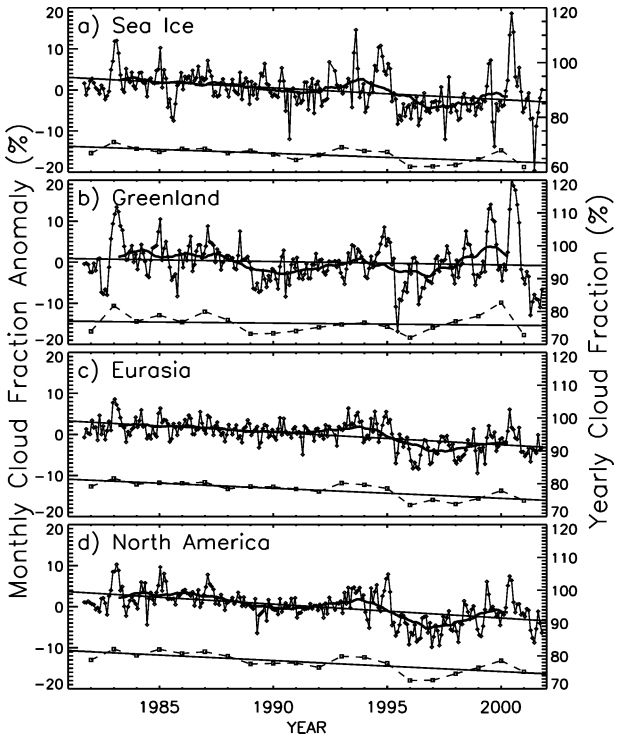

FIG. 10. Monthly anomalies and yearly averages (dash line) of cloud fractions over (a) sea ice, (b) Greenland, (c) Eurasia, and (d) North America.

tration on the temperature trends is not known, and the lack of detailed spatial information about the distribution of different types of aerosol, absorption characteristics of each type, and a good atmospheric model makes it difficult to obtain an accurate assessment. Such a study is not within the scope of this paper. It should be noted, however, that the normalization of the AVHRR data from different sensors, as discussed below, to get them to agree with in situ data minimizes the problem of increasing percentages of aerosol.

b. Sensor calibration

The AVHRR sensors have all been carefully calibrated while on the ground. The characteristics of these sensors, however, are known to change after launch and the unknown accuracies of the onboard calibration system make it difficult to obtain absolute calibration. A check on the consistency of calibrated data from the different sensors used to create the time series is therefore important if not necessary. For lack of a better technique and as is done in SST studies, we use in situ data to improve the calibration of the different AVHRR sensors starting with *NOAA-7* through *NOAA-16.* For each of the sensors, a slight normalization of original calibrated data based on results of regression analysis was made to get the retrieved surface temperatures consistent with in situ surface measurements. This required making assumptions such as a linear relationship between in situ and AVHRR data for all seasons. The scatterplots shown in Figs. 1 and 2 are manifestations that the normalized AVHRR data are temporally consistent for the 1981–2001 period and with the standard deviations and rms errors consistent if not better than expectations.

6. Long-term trends and cyclical patterns from station data

When using satellite data for trend analysis, the concern has been its relatively short record length and how effectively the data represent real trends. To gain insights into this problem, we analyzed the longer-term meteorological station data north of 60°N from 1900 to 2000 compiled by Jones et al. (1999). The averages of monthly surface temperature anomalies, presented in Fig. 11, show that the year-to-year fluctuation is large even with the seasonality subtracted. The 5-yr running averages, shown in gray, are much less variable and show some sinusoidal patterns. The trend in temperature, inferred from the 100-yr record of temperature anomalies is 0.06 ± 0.01°C decade^{-1} while that for the recent 20 yr is 0.48 ± 0.10°C decade^{-1}. The 20-yr trend is about eight times higher than the 100-yr trend indicating a rapidly increasing warming rate. The variability of the trend as a function of record length was also studied as in Comiso (2000) and the results show large fluctuations for record lengths less than 15 yr. Beyond this record length, the trend tends to stabilize and falls off exponentially with time. It thus appears that our satellite record of two decades is long enough for meaningful trend studies.

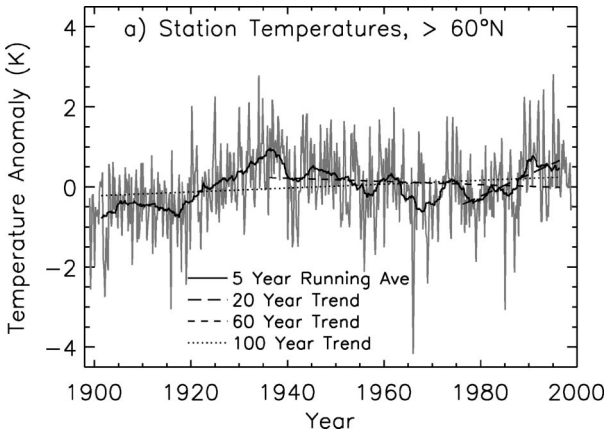

FIG. 11. Monthly anomalies from the 100-yr station record from 1900 to 1999. A dotted line shows a trend of $0.06 + 0.01$°C decade^{-1} for the 100-yr record, a dashed line shows a trend of -0.40 ± -0.07°C decade^{-1} for the last 65 yr, while the dashed line shows 0.48 ± 0.10°C decade^{-1} for the last 20 yr. The bold line represents a 5-yr running mean.

It is interesting to note, however, that the value goes negative at about -0.40 ± 0.07°C decade^{-1} for the 65-yr record that goes from 1936 to 2000. The latter was caused by relatively high temperature values in the 1930s (Fig. 11) as noted previously (Hansen and Lebedeff 1987). This implies that trend results have to be interpreted carefully since a relatively long record of 65 yr provides a trend with opposite sign compared to that of a 100-yr record. Also, the 100-yr record appears low because of the relatively warm temperatures in the 1930s. Spectral analysis using the data in Fig. 11 also shows a peak suggesting a periodic cycle at around 12 yr. This is likely the influence of the interdecadal fluctuations in surface temperature and pressure associated with the Arctic Oscillation (AO; Thompson and Wallace 1998; Rigors et al. 2002) and the North Atlantic Oscillation (NAO; Mysak and Venegas 1998). Detailed correlation analysis of the AO/NAO with the AVHRR data as well as its impact on the observed interdecadal variability in surface temperature is beyond the scope of this paper. It should be noted that the warming trend observed in the last decade has been generally associated with an increasing positive phase of the AO/NAO, which, according to a model experiment by Shindell et al. (1999), is attributed to warming due to enhanced greenhouse gases.

7. Conclusions

Two decades of satellite clear sky thermal infrared data show for the first time spatially detailed distribution of temperature anomalies in the pan-Arctic region from

1981 to 2000. The yearly anomalies are generally negative in the 1980s up to 1988 and generally positive after that. The change from negative to positive coincides with the observed change in phase of the AO. Trend analysis using monthly anomalies and yearly values shows a dominance of positive trends with the high positive values located in the western Arctic, but the spatial variation of this trend is large with negative values in the Greenland ice sheets and parts of Siberia. Quantitatively, the trends based on monthly anomalies (and also yearly means) are, on average, 0.33°C decade^{-1} over sea ice, $-0.09°$ decade^{-1} over Greenland, 1.06°C decade^{-1} over North America, and 0.5°C decade^{-1} over northern Eurasia. Large variations in the monthly anomalies are observed but trend analysis based on yearly averages yields basically identical results.

Seasonally, the trends are mainly positive in summer, spring, and autumn when the impact on frozen surfaces is most critical. Unexpectedly, the trends are observed to be generally negative in winter, with some cooling observed in large areas in the Bering Sea and parts of Russia. The locations of negative trends in winter are consistent with those where positive trends in the sea ice cover have been identified (Parkinson et al. 1999). The length of the melt season is also observed to be increasing from 9 to 17 days decade^{-1} consistent with the apparent warming in the spring, summer, and autumn and suggesting a decreasing volume for the sea ice cover.

A sustained warming of the magnitude observed would cause profound changes in the Arctic region, especially in the sea ice cover, parts of the Greenland ice sheet, the permafrost, glaciers, and snow cover over northern Eurasia and North America. The longer-term station dataset also suggests acceleration in the warming rate but this may in part be caused but abnormally warm temperatures in the 1930s. Spectral analysis of the station data reveals a 12-yr cycle that is likely associated with the AO and NAO. The warming in recent decades has been attributed to increases in the positive phase of the AO/NAO, which in turn has been linked to the enhanced concentration of greenhouse gases in the atmosphere by Shindell et al. (1999), using a stratospheric-resolving climate model. The latter suggests that the observed warming in this study may not be natural in origin despite the observed decadal variability.

Acknowledgments. The author is grateful to Larry Stock for excellent programming and analysis support for this project. He is also very grateful to two reviewers and the editor for useful comments and suggestions. This project is funded by NASA's Cryospheric Sciences Program.

REFERENCES

Bjorgo, E., O. M. Johannessen, and M. W. Miles, 1997: Analysis of merged SSMR-SSMI time series of Arctic and Antarctic sea ice parameters 1978–1995. *Geophys. Res. Lett.,* **24,** 413–416.

Budyko, M. I., 1966: Polar ice and climate. *Proceedings of the Symposium on the Arctic Heat Budget and Atmospheric Circulation,* J. O. Fletcher, Ed., RM5233-NSF, Rand Corporation, 3–21.

Comiso, J. C., 2000: Variability and trends in Antarctic surface temperatures from in situ and satellite infrared measurements. *J. Climate,* **13,** 1674–1696.

——, 2001: Satellite observed variability and trend in sea ice extent, surface temperature, albedo, and clouds in the Arctic. *Ann. Glaciol.,* **33,** 457–473.

——, 2002: A rapidly declining Arctic Perennial Ice Cover. *Geophys Res. Lett.,* **29,** 1956, doi:10.1029/2002GL015650.

Doran, P. T., and Coauthors, 2002: Antarctic temperature cooling and terrestial ecosystem response. *Nature,* **415,** 517–520.

Draper, N., and H. Smith, 1981: *Applied Regression Analysis.* 2d ed. John Wiley and Sons, 709 pp.

Häkkinen, S., and G. L. Mellor, 1990: One hundred years of Arctic ice cover variations as simulated by a one-dimensional, ice-ocean model. *J. Geophys. Res.,* **95** (C9), 15 959–15 969.

Hansen, J., and S. Lebedeff, 1987: Global trends of measured surface air temperature. *J. Geophys. Res.,* **92** (C11), 13 345–13 372.

Honjo, S., T. Takizawa, R. Krishfield, J. Kemp, and K. Hatekeyama, 1995: Drifting buoys make discoveries about interactive processes in the Arctic Ocean. *Eos, Trans. Amer. Geophys. Union,* **76,** 209–215.

Jacobs, S. S., and J. C. Comiso, 1997: A climate anomaly in the Amundsen and Bellingshausen Seas. *J. Climate,* **10,** 697–709.

Johannessen, O. L., E. V. Shalina, and M. W. Miles, 1999: Satellite evidence for an Arctic sea ice cover in transformation. *Science,* **286,** 1937–1939.

Jones, P. D., M. New, D. E. Parker, S. Martin, and I. G. Rigor, 1999: Surface air temperature and its changes over the past 150 years. *Rev. Geophys.,* **37,** 173–199.

King, J. C., and J. C. Comiso, 2003: The spatial coherence of interannual temperature variations in the Antarctic Peninsula. *Geophys. Res. Lett.,* **30,** 1040, doi:10.1029/2002GL015580.

Krabill, W., and Coauthors, 2000: Greenland ice sheet: High-elevation balance and pheripheral thinning. *Science,* **289,** 428–430.

Kwok, R., and J. C. Comiso, 2002: Southern ocean climate and sea ice anomalies associated with the Southern Oscillation. *J. Climate,* **15,** 487–501.

Lemke, P., and M. Hilmer, 2000: On the decrease of Arctic Sea ice volume. *Geophys. Res. Lett.,* **27,** 3751–3754.

Lindsay, R. W., 1998: Temporal variability of the energy balance of thick Arctic pack ice. *J. Climate,* **11,** 313–333.

Manabe, S., M. J. Spelman, and R. J. Stoufer, 1992: Transient responses of a coupled ocean–atmosphere model to gradual changes of atmospheric CO_2. Part II: Seasonal response. *J. Climate,* **5,** 105–126.

McPhee, M. G., T. P. Stanton, J. H. Morison, and D. G. Martinson, 1998: Freshening of the upper ocean in the Arctic: Is perennial sea ice disappearing? *Geophys. Res. Letter.,* **25,** 1729–1732.

Mysak, L. A., and S. A. Venegas, 1998: Decadal climate oscillations in the Arctic: A new feedback loop for atmosphere–ice–ocean interactions. *Geophys. Res. Lett.,* **25,** 3607–3610.

Overland, J. E., M. Wang, and N. A. Bond, 2002: Recent temperature change in the western Arctic during Spring. *J. Climate,* **15,** 1702–1716.

Parkinson, C. L., D. J. Cavalieri, P. Gloersen, H. J. Zwally, and J. C. Comiso, 1999: Arctic Sea ice extends, areas, and trends, 1978–1996. *J. Geophys. Res.,* **104** (C9), 20 837–20 856.

Perovich, D. K., and B. Elder, 2001: Temporal evolution and spatial variability of the temperature of Arctic Sea ice. *Ann. Glaciol.,* **33,** 207–212.

Proshutinsky, A., and M. Johnson, 1997: Two circulation regimes of the wind driven Arctic Ocean. *J. Geophys. Res.,* **102,** 12 493–12 514.

Raper, S. C. B., T. M. L. Wigley, P. D. Jones, P. M. Kelley, P. R. Mayes, and D. W. S. Limbert, 1983: Recent temperature changes in the Arctic and the Antarctic. *Nature,* **306,** 458–459.

Rigor, I. G., R. L. Colony, and S. Martin, 2000: Variations in surface

air temperature observations in the Arctic, 1979–97. *J. Climate,* **13,** 896–914.
——, J. M. Wallace, and R. L. Colony, 2002: Response of sea ice to the Arctic Oscillation. *J. Climate,* **15,** 2648–2663.
Rothrock, D. A., Y. Yu, and G. A. Maykut, 1999: Thinning of the Arctic sea-ice cover. *Geophys. Res. Lett.,* **26,** 3469–3472.
Shindell, D. T., R. L. Miller, G. A. Schmidt, and L. Pandolfo, 1999: Simulation of recent winter climate trends by greenhouse-gas forcing. *Nature,* **399,** 452–455.
Steffen, K., and J. E. Box, 2001: Surface climatology of the Greenland ice sheet: Greenland climate network, 1995–1999. *J. Geophys. Res.,* **106** (D24), 33 951–33 964.
——, and Coauthors, 1993: Snow and ice applications of AVHRR in polar regions: Report of a workshop held in Boulder, Colorado, 20 May 1992. *Ann. Glaciol.,* **17,** 1–16.
Thomas, R., T. Akins, B. Csatho, M. Fahnestock, P. Gogineni, C. Kim, and J. Sonntag, 2000: Mass balance of the Greenland ice sheet at high elevations. *Science,* **289,** 426–428.
Thompson, D. W. J., and J. M. Wallace, 1998: The Arctic oscillation signature in the wintertime geopotential height and temperature fields. *Geophys. Res. Lett.,* **25,** 1297–1300.
Tucker, W. B., III, J. W. Weatherly, D. T. Eppler, D. Farmer, and D. L. Bentley, 2001: Evidence for the rapid thinning of sea ice in the western Arctic Ocean at the end of the 1980s. *Geophys. Res. Lett.,* **28,** 2851–2854.
Wadhams, P., and N. R. Davis, 2000: Further evidence of ice thinning in the Arctic Ocean. *Geophys. Res. Lett.,* **27,** 3973–3976.
Walsh, J. E., W. L. Chapman, and T. L. Shy, 1996: Recent decrease of sea level pressure in the Central Arctic. *J. Climate,* **9,** 480–486.
Zwally, H. J., and S. Fiegles, 1994: Extent and duration of Antarctic surface melting. *J. Glaciol.,* **40,** 463–476.
——, W. Abdalati, T. Herring, K. Larson, J. Saba, and K. Steffen, 2002: Surface melt-induced acceleration of Greenland ice-sheet flow. *Science,* **297,** 218–222.